ISSN 2070-0482, Mathematical Models and Computer Simulations, 2013, Vol. 5, No. 5, pp. 470–478. © Pleiades Publishing, Ltd., 2013.
Original Russian Text © T.G. Elizarova, D.S. Saburin, 2013, published in Matematicheskoe Modelirovanie, 2013, Vol. 25, No. 3, pp. 75–88.

Numerical Simulation of Fluid Oscillations in Fuel Tanks

T. G. Elizarova[a] and D. S. Saburin[b]

[a] *Keldysh Institute of Applied Mathematics, Russian Academy of Sciences, Moscow, Russia*
[b] *Moscow State University, Moscow, Russia*
e-mail: telizar@mail.ru

Received July 5, 2012

Abstract—Fluid oscillations in a closed vessel have been numerically simulated. The statement of the problem corresponds to the situations that arise in the fuel tanks of ice-breaking ships in collisions with ice barriers and movement on the waves. The results are obtained using the regularized shallow-water equations.

Keywords: regularization, shallow-water equations, fluid oscillations in fuel tanks

DOI: 10.1134/S2070048213050050

INTRODUCTION

The study of oscillations of fuel and other fluids contained in tanks of modern icebreakers is of great practical interest. In particular, it allows us to estimate the load on the tank walls when a vessel is moving on the waves, or suddenly stops in a collision with an ice floe [1–3]. The movement of the fluid in the tank is three-dimensional and significantly nonstationary. In the description of such flows, modern software systems are employed based on the Navier–Stokes equations with the application of turbulence models and implemented on parallel computer systems [2, 3]. However, in the cases where the tank is underfilled, the numerical simulation of such a flow can be based on the equations of hydrodynamics in the shallow water (SW) approximation [4], which significantly simplifies the calculations.

In [5], a new method of solving the Saint-Venant, or shallow water equations was proposed and tested based on the smoothing of classical equations over a small time interval. This procedure leads to the emergence of regularizing additives, which ensure the numerical stability of the problem in a wide range of Froude numbers. The generalization of the constructed algorithm to the case of flows involving both the emergence and disappearance of dry bottom areas was performed in [6]. Such situations arise under waves crashing on the shore, in flood flows, and under the oscillations of a fluid in a vessel with a complex-shaped bottom.

The regularizing additives for SW equations have also been obtained based on quasi-gas dynamic (CGD) equations when they are written in the barotropic approximation. Numerical algorithms based on the CGD equations are widely used for solving the hydrodynamics equations of a viscous gas and viscous incompressible fluid; see, for example, monographs [7–10]. In [11] it was shown that smoothing additives may be constructed by averaging the original hydrodynamic equations over a small time interval using special assumptions and limitations.

For SW equations with regularizing terms, there holds the law of nonincreasing total energy, which proves
1 the dissipative character of the constructed regularizer [12]. In [13] a similar result was obtained in the form of rigorous theorems for the above-mentioned system describing the flows above a flat bottom. Here, the uniqueness of the solutions for the linear approximation of the system is also proved. Examples of numerical simulation of flows based on the regularized SW equations are given in [5, 6, 14] and [15].

In this paper, we consider the fluid motion in the symmetry plane of a tank. The problem is solved in a
2 noninertial coordinate system. Calculations are made on the basis of regularized shallow water equations.

1. THE SYSTEM OF SHALLOW WATER EQUATIONS AND THE PROBLEM STATEMENT

A system of shallow water or Saint-Venant equations in the flow form can be represented as

$$\frac{\partial h}{\partial t} + \operatorname{div} hu = 0, \tag{1}$$

$$\frac{\partial (h\mathbf{u})}{\partial t} + \operatorname{div}(h\mathbf{u} \otimes \mathbf{u}) + \nabla \frac{gh^2}{2} = h(\mathbf{f} - g\nabla b) - \mu \mathbf{u}|\mathbf{u}|. \tag{2}$$

The unknown quantities in system (1) and (2) are $h(\mathbf{x},t)$, the height of the fluid level, and $\mathbf{u}(\mathbf{x},t)$, its velocity. Here, the known quantity $b(\mathbf{x})$ designates the mark of the bottom relief, $g = 9.8$ m/s^2 is the acceleration of gravity, $\mathbf{f}$ is the external mass force, and μ is the dimensionless coefficient of hydraulic friction.

We consider a tank containing stationary fluid with the benchmark h_0, i.e., $h(\mathbf{x},0) = h_0$. On the boundaries of the tank we impose impermeability conditions for the velocity and conditions of reflection for the quantity h

$$u = 0, \quad \frac{\partial h}{\partial x_i} = 0.$$

2 The problem is considered in a noninertial frame of reference in which the process of stopping or nonuniform motion of the vessel is described by the action of the mass inertial force $\mathbf{f}(t)$. The value of the force is determined by the law of the time dependence of the vessel speed $\mathbf{V}(t)$ and is calculated as

$$\mathbf{f} = \frac{d\mathbf{V}}{dt}.$$

When the vessel stops due to a collision with an ice floe, force $\mathbf{f}$ acts on the fluid during some specified time interval Δt_0. When the vessel moves on waves the corresponding law of the velocity change is imposed.

In practical situations, the inertia force only acts in the direction of the vessel; i.e., it has only one component directed along the axis of the tank, which is also located along the longitudinal axis of the vessel. Therefore, in this work, the fluid flow is only considered in the symmetry plane of the tank and the problem is only solved in the one-dimensional approximation.

2. REGULARIZED SHALLOW WATER EQUATIONS AND METHOD OF NUMERICAL SOLUTION

For the numerical solution of shallow water equations, we use the regularized form of these equations; see, for example, [5]. For a planar one-dimensional flow, a system of the regularized SW equations has the following form (see, for example, [15]):

$$\frac{\partial h}{\partial t} + \frac{\partial j_m}{\partial x} = 0, \tag{3}$$

$$\frac{\partial hu}{\partial t} + \frac{\partial j_m u}{\partial x} + \frac{\partial}{\partial x}\left(\frac{gh^2}{2}\right) = \left(h - \tau\frac{\partial hu}{\partial x}\right)\left(f - g\frac{\partial b}{\partial x}\right) + \frac{\partial \Pi}{\partial x} - \mu u|u|, \tag{4}$$

where

$$j_m = h(u - w), \quad w = \frac{\tau}{h}\left(\frac{\partial hu^2}{\partial x} + gh\frac{\partial h}{\partial x} + gh\frac{\partial b}{\partial x} - hf\right), \tag{5}$$

$$\Pi = \tau uh\left(u\frac{\partial u}{\partial x} + g\frac{\partial h}{\partial x} + g\frac{\partial b}{\partial x} - f\right) + \tau gh\left(u\frac{\partial h}{\partial x} + h\frac{\partial u}{\partial x}\right) + \tau\frac{gh^2}{2}\frac{\partial u}{\partial x}, \tag{6}$$

where τ is the parameter of regularization or smoothing.

When $\tau = 0$ the system of equations (3)–(6) becomes a classical system of shallow water equations (1)–(2). In the numerical calculations, the terms with the coefficient τ are regarded as regularizing additives.

For the numerical solutions of the regularized shallow water equations, we use a time-explicit difference scheme with the approximation of all spatial derivatives by the central differences. The values of the sought variables $h(x, t)$ and $u(x, t)$ are assigned to the nodes of the spatial grid. The stability of the numerical algorithm is ensured by the terms with coefficient τ, the value of which is connected with the step of spatial grid h_x and is calculated as

$$\tau = \alpha\frac{h_x}{c}, \quad c = \sqrt{gh(x,t)}, \tag{7}$$

where c is the propagation velocity of small perturbations calculated in the approximation of the SW model and $0 < \alpha < 1$ is the numerical coefficient selected on the condition of accuracy and stability of the computation. The time step is selected according to the Courant condition, which for this problem has the form

$$\Delta t = \beta(h_x/c)_{\min}. \tag{8}$$

Here, the coefficient $0 < \beta < 1$ depends on the value of the regularization parameter τ and is selected in the course of the calculations, in order to ensure the monotonicity of the numerical solution. The difference algorithm for the solution of the system of equations (3)–(6) is presented, for instance, in [15, 14]. In the calculations uniform spatial grids were employed.

3. VESSEL STOPPING IN ITS COLLISION WITH AN ICE FLOE

The problem was solved in statement [3]. The length of tank L ranged from 30 m to 40 m, the initial height of level h_0 did not exceed 3 m. In the symmetry plane the tank had a flat bottom $b(x) = \text{const}$. The coefficient of hydraulic friction μ took the values 0 and 0.001. The vessel's speed V is assumed to be directed along the axis x. The pattern of the speed variations in a gas carrier vessel at its collision with an ice barrier is described by polynomials of the sixth degree [3]. For the initial speed of the vessel equal to 8 knots, this polynomial has the form

$$V = -6.8192t^6 + 22.639t^5 - 7.693t^4 - 12.453t^3 + 0.1757t^2 - 0.0249t + 4.1161, \quad (9)$$

for the initial speed of the vessel equal to 6 knots

$$V = -2.4914t^6 + 9.3244t^5 - 3.5721t^4 - 6.5188t^3 + 0.1037t^2 - 0.0165t + 3.0871, \quad (10)$$

and for the initial speed of the vessel equal to 4 knots

$$V = -0.6027t^6 + 2.671t^5 - 1.2116t^4 - 2.618t^3 + 0.0493t^2 - 0.0093t + 2.0581. \quad (11)$$

One nautical knot is equal to 0.514 m/s. In the above formulas, the speed is measured in meters per second. Further, all values are given in the International System of Units (SI system). Velocity-time diagrams are presented in Fig. 1. The diagrams clearly show that for all three variants the vessel stops in about one second.

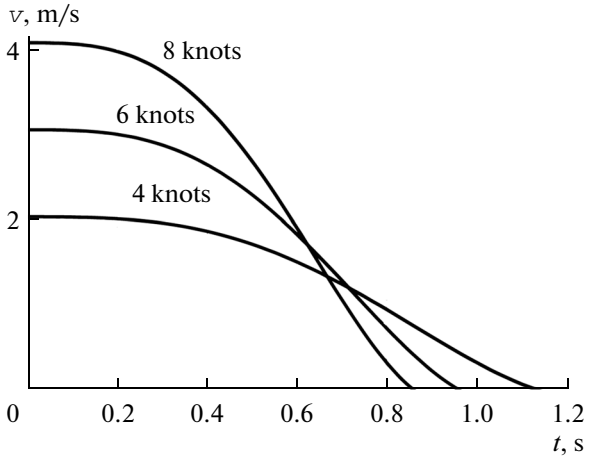

Fig. 1. Examples of the evolution of the vessels speed as it stops.

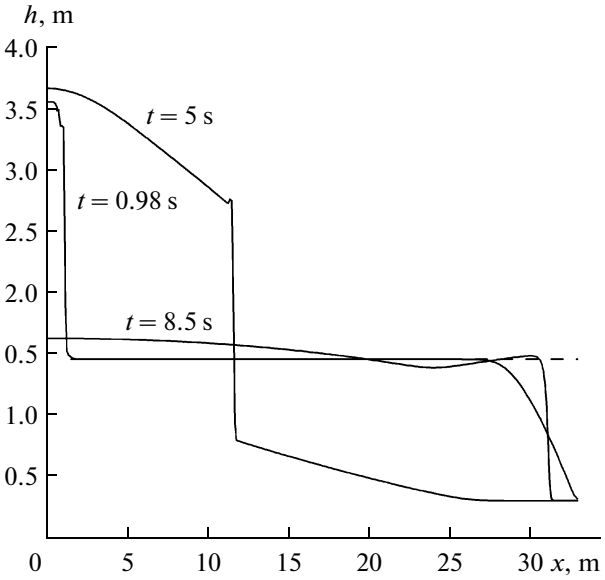

Fig. 2. The fluid level for successive time instants, $h_0 = 1.46$ m.

General Flow Pattern. We will dwell on the calculation variant where the initial speed of the vessel is 8 knots, the length of tank $L = 33.6$ m, and the initial height of fluid $h_0 = 1.46$ m.

Figure 2 shows the position of the fluid level $h(x)$ for four successive time instants 0, 0.98, 5, and 8.5 s. A characteristic fluid blowout up the front wall of the tank is clearly visible, as well as the gradual lowering of the level over time. Figure 3 shows the corresponding distributions of the fluid velocity in the tank. In the both graphs there are pronounced large gradients in the distributions of speed and height. At these times the Froude number $\mathrm{Fr} = |u|/c$ reaches the value of 1.1, which corresponds to the supercritical flow characteristic of the formation of discontinuous solutions such as a hydraulic jump.

From the practical standpoint, the value of the load on the tank walls as the vessel stops is of interest. The pressure in tank P is calculated as $P(x,t) = P_{atm} + gh(x,t)\rho$, where ρ is the fluid density and P_{atm} is the atmospheric pressure, including the pressure of the fluid's vapor.

A fragment of the plotted pressure fluctuations on the front wall of the tank is shown in Fig. 4 for the calculation variant $L = 36.5$ m, $h_0 = 2.86$ m, and $\mu = 0$. Here, $\rho = 700$ kg/m^3 and $P_{atm} = 101$ kPa. At the beginning of the process, the variations have an irregular form but with the passage of time weakly attenuating harmonic oscillations are established that are smoothed at times of the order of 700 s. For times $100 < t < 500$, fluid oscillations in the tank are close to harmonic. Due to the reflection condition, the tank's length L accommodates half of the wavelength of the main frequency mode $\lambda = 2L$. Thus, the period of oscillation is connected with the wave velocity by the relation

$$T = \frac{2L}{c}. \quad (12)$$

In [4] (on page 60), an analytical formula is given for the propagation velocity of a gravitational wave on the surface of the fluid of unlimited depth h_0

$$c = \frac{\sqrt{g}}{2\sqrt{k\tanh(kh_0)}}\left(\tanh(kh_0) + \frac{kh_0}{\cosh^2(kh_0)}\right). \quad (13)$$

For this calculation, the depth of the fluid in tank $h_0 = 2.86$ m and the wave number $k = 2\pi/\lambda = \pi/L$. Thus, $kh_0 = 0.24$, which roughly corresponds to the long-wave approximation $kh_0 \ll 1$. In this approximation, expression (13) is simplified and assumes the form $c = \sqrt{gh_0}$.

According to (12) and (13), the value of the oscillation period in the case is $T = 14.26$ s. The use of long-wave approximation yields the value $T = 13.86$ s. In the above calculation, the oscillation period is 14 ± 0.45 s when it is measured in the time interval $30 < t < 550$ s. The obtained value corresponds to the theoretical estimates based on the value of the propagation velocity of a gravitational wave in the fluid.

Thus, for a specified period of time we can talk about the numerical solution attaining an analytical dependence, which is consistent with the hydrodynamic description of the oscillation process. This confirms the physical nature of dissipation in the finite-difference algorithm used by the authors.

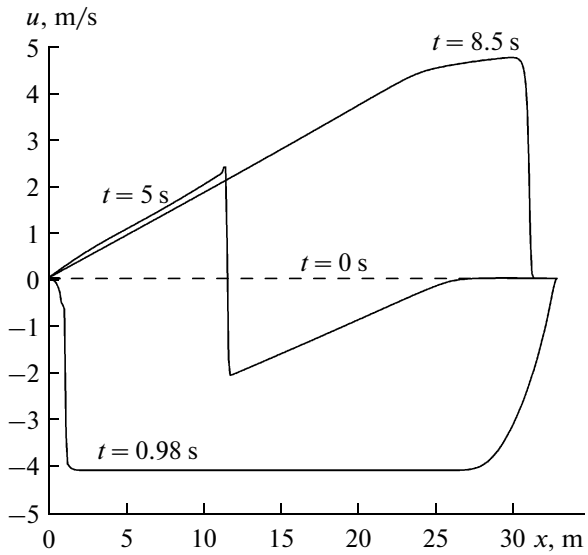

Fig. 3. Speed distribution for successive time instants, $h_0 = 1.46$ m.

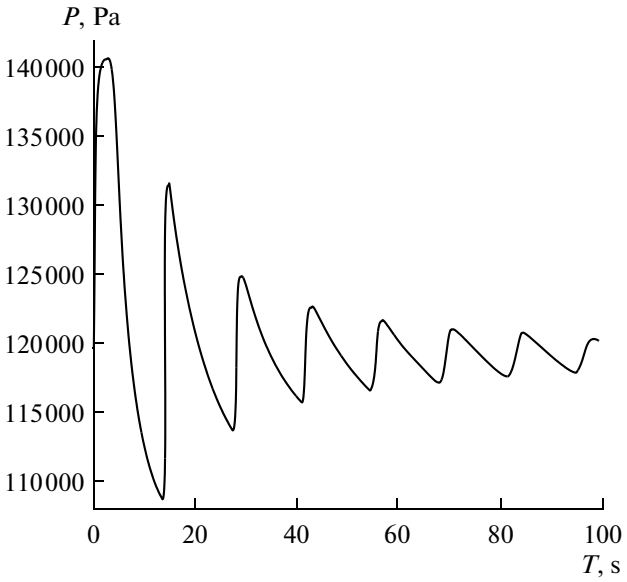

Fig. 4. Plotted time dependence of the load on the front wall, fragment 0–100 s, level height $h_0 = 2.86$ m, speed 8 knots.

Comparison with Calculations by a Three-Dimensional Model. A detailed study of fluid oscillations in a tank of a gas carrier vessel is given in [3], where the spatial nonstationary flow arising when the vessel stops is calculated on the basis of the time-averaged Navier–Stokes equations in the form of Reynolds equations in order to allow for the turbulence effect (URANS model). The problem was solved in the approximation of an incompressible viscous fluid taking into account the changes in the shape of the surface. For the numerical solution of the problem, the finite-element method, adapted to use on high-performance parallel computer systems, was employed. The latter is necessary for solving this highly computationally cumbersome problem. Because of the computational complexity, and taking into account the practical considerations, calculations were made up to the time of the order of 20 s. In [3], the flows are calculated for the vessel stopping for the case of the tank filled to an arbitrary level but there is also the calculation for the tank filled to ten percent of its capacity. In the latter case, height h_0 is 1.46 m, which is significantly less than the tank length. The approximate data about such a flow in the tank can be obtained by the shallow water equations.

The results of the calculation within the frame of the SW equations are given in Fig. 5, which presents the time variation graphs for the pressure on the front and back walls of the tank during the first 20s. The initial the vessel speed is 8 knots, the initial fluid height is 1.46 m, and the value of the friction coefficient is $\mu = 0.001$. Figure 6 presents the corresponding graphs obtained in [3] for two points located at the bottom of the front and back walls of the tank.

The comparison of the graphs presented above shows that despite the limitations of the shallow water approximation model, the main features in the distribution of the load on the front and back walls of the tank

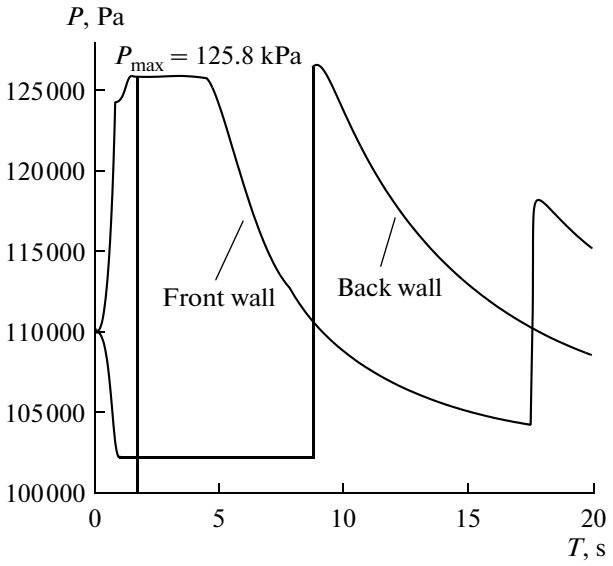

Fig. 5. Time dependence of the pressure on the front and back walls of the tank, fragment 0–20 s, speed 8 knots, level height $h_0 = 1.46$ m.

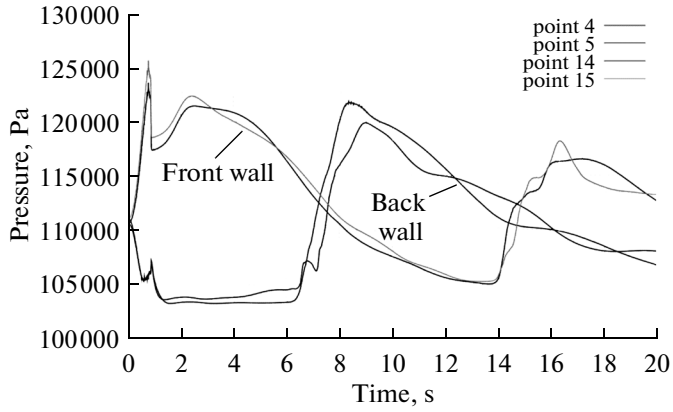

Fig. 6. The same, calculated by URANS model [3].

are represented with sufficient accuracy. In particular, both calculations yield similar maximum and minimum values of the pressure on these walls and there is satisfactory agreement between the time instants corresponding to the run-up and sweep-back of the wave of pressure on the front and back walls of the tank. Indeed, for the front wall of the tank, the arrival time of the first pressure wave for both models is ~17.5 and 16 s for models SW and URANS, respectively. For the back wall, the time of the back-sweep of the pressure wave for both models is ~1 s, and the arrival time of the pressure wave is calculated as ~9 and 8 s for the SW and URANS approximations, respectively.

It should be noted that this calculation in the approximation of the shallow water equations takes a few minutes on a personal computer, which is significantly less than the costs required to compute the problem in its complete statement [3].

The plotted distribution of the load on the tank walls for vessel speeds of 6 and 4 knots is shown in Fig. 7. It can be seen that when the initial speed of the vessel is decreased both the minimum and maximum loads on the tank walls are reduced and the duration of the maximum load is increased. The latter is clear from the widened maximum on the plotted load on the back wall of the tank. Moreover, as the initial speed decreases, the arrival time for the respective waves of the pressure on the walls is somewhat increased. Our calculations also show that with the increase in tank length L and decrease in the initial height of the fluid level h_0, the arrival time for the second peak of the pressure on the front and back walls of the tank is increased. The smoothing effect of the friction coefficient on the pressure gradient appears to be negligible.

Table 1 shows the ratios of the maximum load on the front tank wall calculated for the above-mentioned three modes of the vessel motion within the context of the shallow-water equations and the URANS model [3].

The presented table demonstrates a good quantitative agreement between the results obtained by approximate and more accurate models, simulating the process for the maximum loads on the tank wall for all three modes of the vessel stopping in the water.

The above-presented calculations were made on a spatial grid with $h_x = 0.1$ m; time step $\Delta t = 0.0026$ s, which corresponds to the Courant number $\beta = 0.1$; and the regularization parameter τ calculated by formula (7) for $\alpha = 0.1$. At lower values of α, there are numerical oscillations arising in the solution that can be eliminated by reducing the time step. Calculations on grids with the steps of 2 m, 0.5 m, and 0.1 m were virtually indistinguishable, indicating that the convergence of the numerical solutions has been achieved with respect to the grid.

Formation of Dry Bottom Areas. Investigating the process of the formation of dry bottom areas in a tank is an important aspect of our problem in terms of estimating the mechanical loads on the bottom surface and walls of the tank. The term *dry bottom* means the formation or the presence of areas with a zero fluid level in the tank. In order to calculate problems where dry bottom areas can arise, the above-described algorithm is modified in the following way: if at some spatial point i on a new time layer the fluid level h_i has become lower

than a certain fixed value ε, then at this point on a new time layer the values of the fluid velocity u_i and the regularization parameter τ are assumed to be equal to zero [6].

For the problems of a vessel stopping at the collision with an ice barrier, calculations were made for all three initial speeds, the tank length of 33.6 m and for the tank filled to various levels in order to find the level of the tank at which dry bottom areas can be formed. The minimum height accepted for calculating the dry bottom, was $\varepsilon = 0.001$ m. Table 2 gives the maximum values of the fluid level in the tanks, at which a dry bottom can emerge, for all three initial speeds. Here, the maximum values of the Froude number are presented obtained by the above-described calculations.

We consider the formation process of the dry bottom area using the example of the calculation variant with the initial speed of 8 knots and $h_0 = 0.53$ m. At the initial instants the general form of the solution corresponds qualitatively to Fig. 2, except that in the right-side area by the time instant ~5 s level h drops to zero.

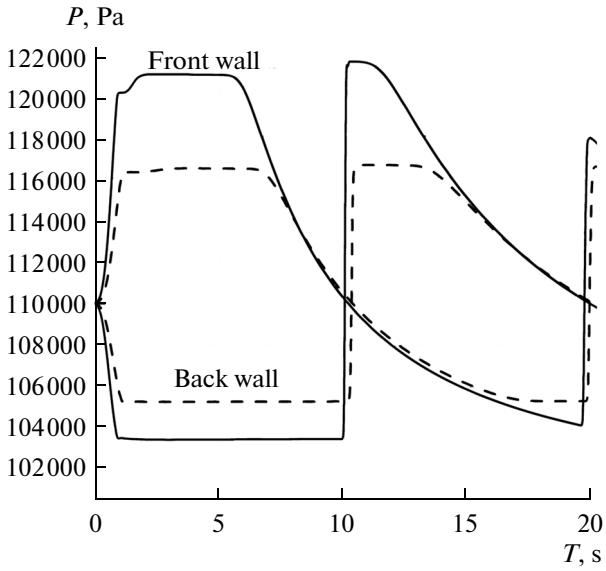

Fig. 7. The pressure on the front wall of the tank, initial level height $h_0 = 1.46$ m, speed of 6 knots (solid line) and speed of 4 knots (dashed line).

The formation of the dry bottom areas in itself does not lead to computational instabilities but the formation of areas with a low fluid level, $h > \varepsilon$, at certain times is accompanied by a sharp increase in the local Froude number, which can result in the instability of the numerical solution. The causes for the emerging high values of Fr are obvious from Fig. 8. Indeed, value Fr sharply increases with the wave reflected from the left wall moving rightwards when the fluid level in the vicinity of the right wall is rather low but higher than ε. Moreover, large values of Fr are maintained not longer than 5 s, and the numerical solution does not lose its stability. When the calculation is continued, the values of Fr do not exceed 2. The parameters of the algorithm for this variant were $\alpha = 0.3$ and the Courant number $\beta = 0.01$. At a further decrease in the level h_0 to which the tank is filled, these processes are manifested more intensively. The stability of the numerical algorithm is sharply improved with an increase in the value of ε.

For a more accurate solution of the problem with a low initial fluid level the employed mathematical model must be supplemented by a more accurate allowance for the hydraulic friction comprising the real values of the Manning factor.

Table 1. The maximum values on the front wall of the tank. Calculated using SW equations with $\alpha = 0.1$

Speed	8 knots	6 knots	4 knots
URANS model	125 kPa	121 kPa	117 kPa
Shallow water equations	125.8 kPa	121.5 kPa	116.6 kPa

Table 2. The maximum values of the fluid level corresponding to the emergence of dry bottom areas and the respective maximum Froude numbers

Speed	8 knots	6 knots	4 knots
The maximum fluid level	0.53 m	0.31 m	0.15 m
The maximum Froude number	10.7	8.21	4.92

4. VESSEL WOBBLING ON THE WAVES

In studying how the wave load affects the behavior of the fluid in the tank it is first assumed that at the initial moment the vessel is motionless and the fluid in the tank is at rest, then the vessel's speed varies pro-

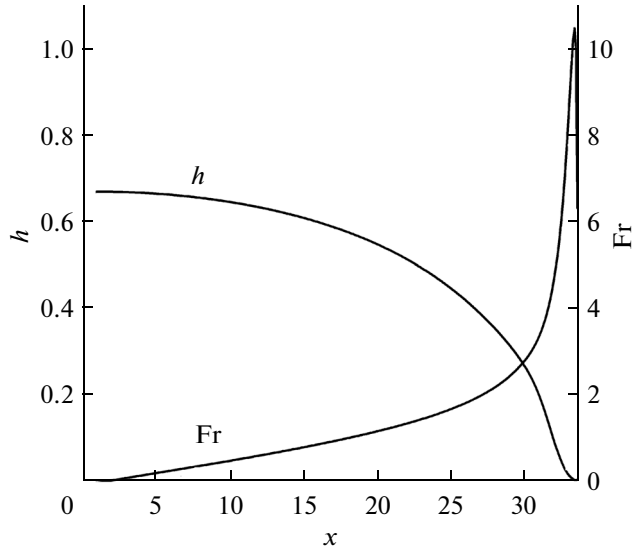

Fig. 8. Distribution of the fluid height h and the Froude number Fr for the initial height $h_0 = 0.53$ m and the initial speed of 8 knots at time instant $t = 11$ c.

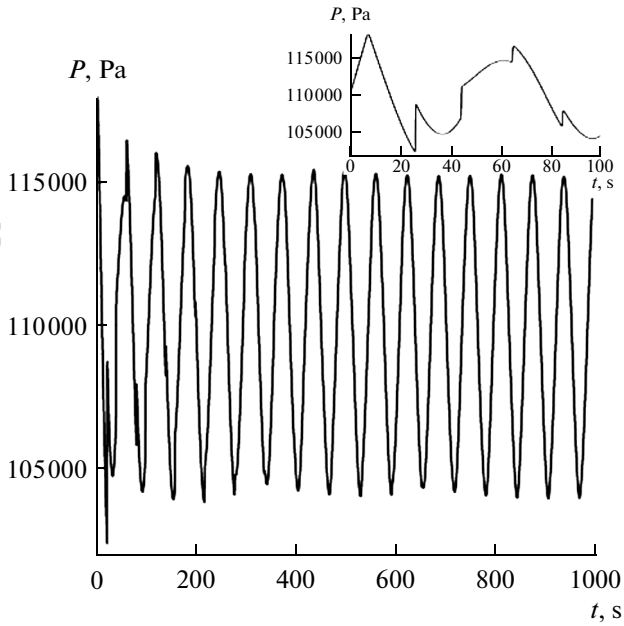

Fig. 9. The pressure on the front wall of the tank as the vessel wobbles on the waves, period $T_1 = 60$ s. At the top we see fragment of the graph at the initial time instant.

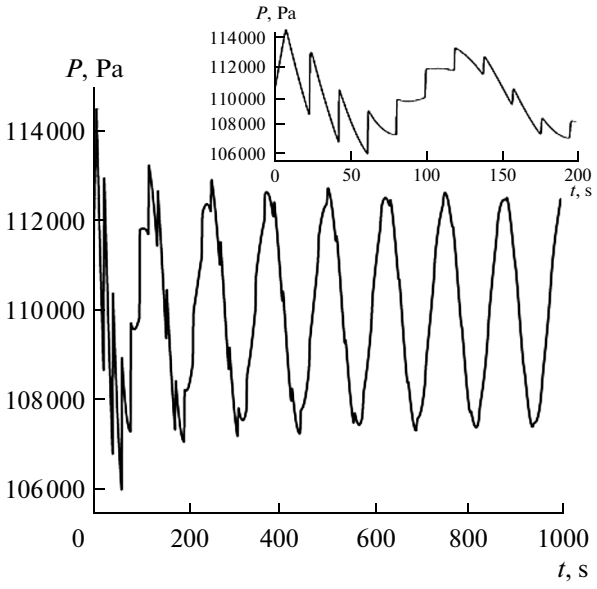

Fig. 10. The same, period $T_2 = 120$ s.

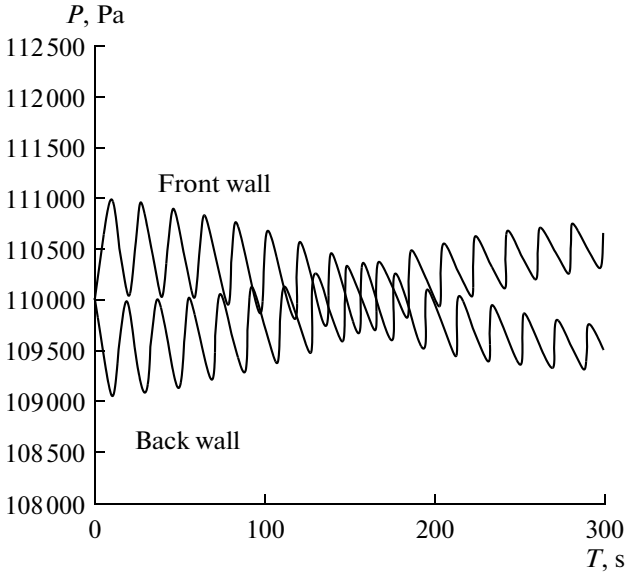

Fig. 11. The pressure on the front and back walls, $T_3 = 600$ s, time interval is 0–300 s.

portionally to $\sin(\omega t)$. Thus, the density of the inertia force can be represented as

$$f(t) = -V\omega\cos(\omega t), \quad \omega = \frac{2\pi}{T}, \tag{14}$$

where T is the given oscillation period and V is the characteristic speed. For practical applications, oscillations with periods $T_1 = 60$ s, $T_2 = 120$ s, $T_3 = 600$ s, and $V = 8$ knots are of interest.

The calculation of these three variants was made for tank length $L = 33.6$ m and initial height of level $h_0 = 1.46$ m on a spatial grid with step $h_x = 0.1$ m for the calculation parameters $\alpha = 0.1$ and $\beta = 0.1$.

Figure 9 presents the time dependence of the pressure on the front wall of the tank for the oscillation period $T_1 = 60$ s. The fragment of the graph shows the evolution of the pressure on the front and back walls of the tank during the first 20 s. It is clear from the figure that the main load on the walls occurs at the first

Table 3. The maximum values on the front wall tank when the ship is bouncing on the waves

Wave period	60 s	120 s	600 s
Maximum pressure	118 kPa	114.5 kPa	111 kPa

time instant with oscillations being highly irregular. They are over time transformed into oscillations with the frequency of the driving force. The corresponding patterns of the loads on the walls for the wave periods T_2 and T_3 are shown in Figs. 10, 11, and 12, respectively. In the last two graphs that correspond to the oscillation period T_3, there is a clearly apparent imposition of natural oscillations in the tank on the oscillations with the frequency of the driving force.

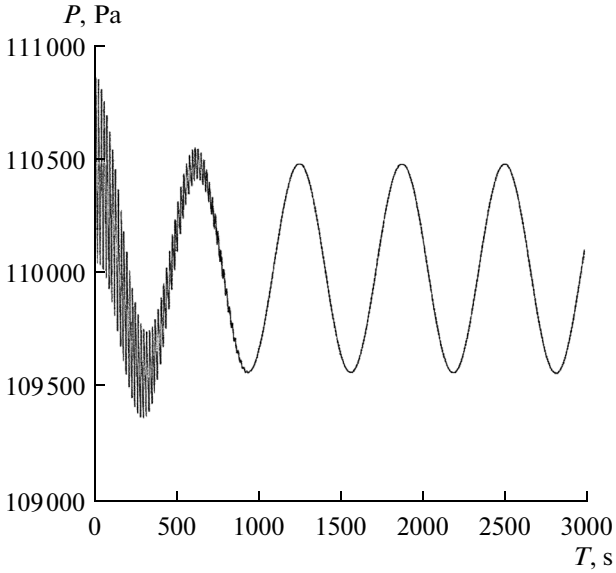

Fig. 12. The pressure on the front wall, $T_3 = 600$ s, time interval 0–3000 s.

Table 3 shows the values of the maximum loads on the front wall of the tank calculated for three variants of wave oscillations of the vessel. The resulting values of the loads obtained by the calculations are of interest for practical applications.

CONCLUSIONS

The mathematical model presented in this work is intended for the description of nonstationary fluid motions in the tanks of cargo ships moving with significant changes in speed. The model is based on the shallow water approximation, which limits the consideration of tanks with a relatively low level of filling.

The numerical algorithm is based on the finite-difference solution of regularized shallow water equations. The regularized shallow water equations themselves and numerical algorithms for their solution are closely related to the earlier studied approach to solving the problems of hydrodynamics on the basis of quasi-gasdynamic equations. The algorithm can be generalized to three-dimensional shallow water flows of the tanks with an arbitrary shape of the bottom.

The shallow water model simplistically describes the complex processes of the fluid's motion in the tank, but the obtained data on the spatial and temporal loads on the walls of the tank are in good agreement with those obtained previously for this problem in the three-dimensional calculations based on the numerical solution of the Reynolds equations with the free boundary of the fluid. Obviously, the solution of the problem in the full statement is a complex and computationally cumbersome problem.

The approach proposed by the authors enables a significant reduction in the computational costs and makes it possible to perform long-time computations for various speed modes, for instance, for the vessel motion on the waves.

The calculations yielded the values of the initial fluid levels under which dry-bottom areas can be formed. It was found that the calculations for low fluid levels are more complex due to the large values of the Froude number in this situation.

The reasonably accurate calculation of the basic characteristics of the process, combined with the simplicity of the numerical algorithm within the shallow water model, makes the approach developed by the authors promising for the quick assessment of the maximum loads on the tank walls of ships in varying navigation conditions. Such data are the most important for practical application in determining the safe speed limits for a ship.

ACKNOWLEDGMENTS

This work was supported by the Russian Foundation for Basic Research, project no. 10-01-00136.

REFERENCES

1. Yu. V. Gur'ev, I. V. Tkachenko, and E. I. Yakushenko, "Computer technology in naval hydrodynamics: status and prospects," Fundam. Appl. Hydrophys., **4** (3), 2011, pp. 8–21.
2. A. S. Safrai and I. V. Tkachenko, "Numerical simulation of gravitational fluid flows in inclined channels," Izv. Ross. Akad. Nauk, Mekh. Zhidk. Gaza, No. 1, 2009, pp. 27–38.
3. A. O. Dukarskii, D. B. Kisilev, I. V. Tkachenko, V. N. Tryaskin, N. V. Tryaskin, and V. V. Yakimov," Mathematical modeling of fluid oscillations in the LNG cargo tanks in a collision with an ice barrier," Morsk. Int. Tekhnol., No. 4, 2011, pp. 69–75.
4. L.D. Landau, and E. M. Lifshits, *Fluid Mechanics* (Butterworth-Heinemann, Oxford, 1987)
5. O. V. Bulatov and T. G. Elizarova, "Regularized shallow water equations and efficient method for the numerical simulation of flows in shallow water," Zh. Vychislit. Matem. Matem. Fiz. **51** (1), pp. 170–184 (2011).
6. O. V. Bulatov and T. G. Elizarova, "Regularized shallow water equations in numerical modeling of tsunami propagation and runup," *Joint Conference Proceedings, 9th International Conference on Urban Earthquake Engineering / 4th Asia Conference on Earthquake Engineering* (Tokyo Inst. Technol, Tokyo, 2012) pp. 2017–2025
7. T. G. Elizarova, *Quasi-Gasdynamic Equations and Methods for Calculation of Viscous Flows* (Nauch. mir, Moscow, 2007) [in Russian].
8. Yu. V. Sheretov, *Continuum Dynamics under Space-Time Averaging* (NITs Reg. Chaot. Dyn., Moscow/Izhevsk, 2009) [in Russian].
9. B. N. Chetverushkin, *Kinetic Schemes and Quasi-Gasdynamic System of Equations* (Maks Press, Moscow, 2004) [in Russian].
10. A. V. Zherikov, *The Use of Quasi-Hydrodynamic Equations, Mathematical Modeling of the Flow of a Viscous Incompressible Fluid* (Lambert Acad. Publ., Saarbrucken, 2010).
11. T. G. Elizarova, "Time averaging as an approximate method for constructing quasi-gasdynamic and quasi-hydrodynamic equations," Zh. Vychislit. Matem. Matem. Fiz. **51** (11), pp. 2096–2105 (2011).
12. A. A. Zlotnik, "Spatial discretization of a one-dimensional barotropic quasi-gasdynamic system of equations and the equation of energy balance," Math. Models Comput. Simul. **24** (10), pp. 51–64 (2012).
13. A. A. Sukhomozgii and Yu. V. Sheretov, "The uniqueness of the solutions of regularized Saint-Venant equations in the linear approximation," Vestn. Tver Univ., Ser. Prikl. Mat., No. 1, pp. 5–7 (2012).
14. T. G. Elizarova, A. A. Zlotnik, and O. V. Nikitina, "Simulation of one-dimensional shallow water flows on the basis of regularized equations," Preprint No. 3, Keldysh Institute of Applied Mathematics, Russian Academy of Sciences (2011).
15. T. G. Elizarova, M. A. Istomina, and N. K. Shelkovnikov, "Numerical simulation of the formation of a solitary wave in the annular aerial hydraulic canals," Math. Models Comput. Simul. **24** (4), pp.107–116 (2012).

Translated by I. Pertsovskaya

SPELL: 1. regularizer, 2. noninertial